World Journal of Advanced Research and Reviews
eISSN: 2581-9615 CODEN (USA): WJARAI
Cross Ref DOI: 10.30574/wjarr
Journal homepage: https://wjarr.com/

(RESEARCH ARTICLE)

Check for updates

A PHYSICS-BASED SIMULATION FRAMEWORK FOR DESIGNING AND TESTING DIGITAL PULSE PROCESSING CHAINS FOR LOW-COST NAI(TL) GAMMA-RAY SPECTROMETRY: DESCRIPTION AND VERIFICATION

Uzo Anekwe, Humphrey Ayodele Peleyeju * and Chibuzo Emeruwa

Department of Physics, Federal University Otuoke, Bayelsa State, Nigeria.
* Corresponding Author

ORCID Details
Humphrey Ayodele Peleyeju: https://orcid.org/0009-0004-9043-9072
Uzo Anekwe: https://orcid.org/0000-0003-0554-8617
Chibuzo Emeruwa : https://orcid.org/0009-0009-9401-9194

World Journal of Advanced Research and Reviews, 2026, 32(02), 930–941

Publication history: Received on 05 October 2026; revised on 11 November 2026; accepted on 13 November 2026

Article DOI: https://doi.org/10.30574/wjarr.2026.32.2.2908

Copyright © 2026 Author(s) retain the copyright of this article. This article is published under the terms of the Creative Commons Attribution License 4.0

ABSTRACT

Routine gamma-ray monitoring of naturally occurring radioactive material in oil-producing regions is limited by the cost of spectrometers, and digital pulse processing moves much of that cost from electronics into software that must then be designed for a noisy, inexpensive front end. Designing it normally requires a detector, and recorded waveforms do not reveal which events a processing chain missed or merged. We describe an open, seeded simulation framework in which a physics-based model of a sodium iodide scintillator, photomultiplier and charge-sensitive preamplifier, calibrated to a published resolution of 6.5 % at 662 keV, feeds a processing chain built from established techniques: recursive trapezoidal shaping with exact pole-zero cancellation, a gated baseline restorer, a fast trigger with hysteresis and second-rise pile-up detection. Because the energy and arrival time of every event are known, each stage can be scored against ground truth. The framework is verified against its design: the modelled pulse has the specified shape, the shaper reproduces its closed-form amplitude calibration and slow-signal response, and the baseline restorer's centred and trailing estimates follow the published 40 and 20 decibel-per-decade prediction. All results are from modelled signals; the model has not been compared with recorded detector waveforms. The measured limits and performance of the chain are reported separately.

Keywords: Digital pulse processing; Gamma-ray spectrometry; NaI(Tl) scintillator; Simulation framework; Trapezoidal shaping; Baseline restoration

1 INTRODUCTION

1.1 Monitoring need

Oil and gas extraction concentrates naturally occurring radionuclides in scale, sludge and produced water, so oil-producing regions need routine gamma-ray monitoring of this technologically enhanced naturally occurring radioactive material (TENORM). In the Niger Delta of Nigeria, the need is documented. Produced water from seven flow stations in Delta State had mean activity concentrations of 48.78 ± 13.67 Bq/L for ^{40}K, 6.04 ± 2.48 Bq/L for ^{226}Ra and 5.18 ± 2.14 Bq/L for ^{228}Ra, all above the World Health Organization limits the authors quote [1], and soil and sludge from ten oil and gas fields had mean activities 48–71 % above a control soil from a non-oil-bearing village, although their radiation hazard indices stayed below permissible limits [2]. Drinking water has been assessed in the same way: the ^{226}Ra, ^{232}Th and ^{40}K content of borehole water from twenty communities in Ogbia, Bayelsa State, was found to carry radiological health risks within safe limits [3]. A regional review notes that equipment for measuring radioactivity in environmental samples is generally scarce in the country, and that nuclear analytical techniques remain relatively elementary partly because of equipment cost [4]. Identifying the radionuclides requires gamma-ray spectrometry; the detector modelled here is a NaI(Tl) scintillator.

1.2 Where the cost lies

In a digital spectrometer the preamplifier output is digitised early and all shaping, triggering and pile-up handling are done in software or firmware [5, 6]. The processing electronics then reduces to an analogue-to-digital converter and a processor. A field-programmable gate array analyser with the same processing stages has been built for an estimated US$300, against US$22 362 for a system built on National Instruments hardware [7], and a sound-card analyser has been described as zero-cost [8]. The cost then sits in the detector and the analogue front end, and a cheaper front end can be expected to be noisier; that expectation, not a measured circuit, is the basis of this paper's low-cost front end. The processing chain must be designed for that front end, which means choosing its filter lengths, trigger levels, pile-up logic and baseline restorer to suit a noise level and count rate that differ from those of laboratory systems.

1.3 The problem this paper addresses

Designing and testing such a chain needs signals to test it on. Waveforms recorded from a detector do not carry the true energy and arrival time of each event, so a chain tested on them can be checked only in aggregate, for example by the width and position of known lines, and not event by event: which pulses it missed, merged or mis-measured, and why. Recording them also needs the detector, front end and digitiser that a resource-limited laboratory may not yet have. A physics-based model of the front end, in which every event's energy and arrival time is known, removes both limitations: each stage of the chain can be scored against ground truth, and the chain can be developed before the hardware exists. The model must then be calibrated and verified carefully enough that its results can be trusted, and its limits stated.

The count rates that matter are modest. For a 3″ × 3″ NaI(Tl) detector held 1 m above ground, the dose rates of a survey across Vietnam correspond to roughly 140–1550 counts per second *(own calculation from the fitted conversion factor and dose rates of [9])*, and count rate falls with crystal size [10].

1.4 Background and related work

Shaping. The chain is built on the recursive trapezoidal filter of Jordanov and Knoll, which synthesises a trapezoid from running sums of a digitised preamplifier signal and folds the cancellation of the preamplifier's exponential decay into a single parameter M [5]. A companion paper gives the same recursion in delay-subtract form, the exact discrete pole-zero parameter $M = 1/\left(e^{T/\tau} - 1\right)$, and notes that the M stage acts as a digital pole-zero canceller [11]. Jordanov later showed that a sampled exponential is unfolded into an impulse scaled by $1/\left(1 - e^{-T/\tau}\right)$ [12], which for the exact M is $M + 1$; this is the origin of the amplitude calibration used here.

Noise and shaping time. The equivalent noise charge of a shaped preamplifier signal has a series (voltage) term that falls with shaping time, a parallel (current) term that rises with it, and a $1/f$ term independent of it, so the optimum lies where the first two are equal [13]. In a well-designed NaI(Tl) system photoelectron statistics dominate the electronic noise [13]. The two front ends modelled here are chosen so that this holds for one and not the other.

Event detection and pile-up. Modern digital spectrometers separate a short fast filter, used for timing and pile-up inspection, from the slow energy filter [6]. Triggering on the slow filter makes the crossing time depend on pulse height (time walk) [13]; timing at a fixed fraction of the pulse height removes this for pulses of constant shape [14]. A pile-up detector that looks for a fall by more than a noise-set margin followed by a renewed rise, while the signal is still above threshold, was described by Mott for the preamplifier slope [15]. Manton notes that pile-up is rarely detected when a pulse arrives on the rising edge of another [16]. Pile-up (pulses summed) and dead time (pulses lost) are distinct effects, and real systems lie between the paralysable and non-paralysable dead-time models [17]; a rejection rule that discards

any event with a neighbour inside a fixed window converts the first into the second and behaves as an extendable (paralysable) dead time, whose throughput is exponential with an effective dead time equal to the interval inspected before and after each event [18].

Baseline restoration. A shaper whose weight function has non-zero area, such as a trapezoid, does not reject a constant input current [19], and deconvolution before a trapezoid reduces an offset or a drift without removing it [20]. The noise cost of restoring the baseline has been analysed from Radeka's closed-form penalty for analogue restorers [21] to optimum digital restorers [19, 22, 23].

Low-cost digital spectrometers. Digital multichannel analysers have been built on PC sound cards, whose 48–192 kHz sampling limits them [7, 8, 24], on an FPGA with a 100 MS/s ADC [7], and on a low-cost 32-bit microcontroller running essentially the same recursive trapezoidal algorithm in real time, for alpha spectroscopy [25]. The last is the closest to this work. It suppresses slow drift inside the filter with a leakage factor slightly below one, whose working range was found by experiment [25], whereas the chain here keeps the filter leak-free and removes slow signals in a separate restorer. That work is evaluated on hardware against a reference acquisition system; the chain here is evaluated on modelled signals only, which gives up comparison with a real detector but allows every stage to be scored against the known energy and arrival time of every event.

1.5 Contributions

This paper describes and verifies such a framework. Its contributions are:

- an open, seeded, physics-based model of a NaI(Tl)/photomultiplier/charge-sensitive-preamplifier front end, calibrated to a published energy resolution, with two front ends that differ only in electronic noise;
- a digital pulse-processing chain built from established techniques (recursive trapezoidal shaping with exact pole-zero cancellation, a gated baseline restorer, a fast trigger with hysteresis re-arm, and second-rise pile-up detection);
- verification of the chain against ground truth, against closed-form results for this recursion, and against the published prediction for centred and trailing baseline estimates.

Every result is obtained from modelled signals; none uses waveforms recorded from a physical detector. The measured limits of the trigger and the baseline restorer, and the chain's performance against peaking time and count rate, are reported separately.

2 MATERIALS AND METHODS

2.1 The synthetic signal source

2.1.1 Forward model

The signal source models a NaI(Tl) scintillator, photomultiplier tube (PMT) and charge-sensitive preamplifier stage by stage, so that the deposited energy and arrival time of every event are known exactly. Figure 1 shows the model and the processing chain as blocks. A fraction of interactions deposits the full gamma-ray energy; the rest are single Compton scatters whose recoil energy is sampled from the Klein–Nishina cross-section up to the Compton edge. The deposited energy produces a Poisson-distributed number of scintillation photons about a mean set by the light yield. Photons are converted to photoelectrons by binomial thinning, first by light-collection efficiency and then by photocathode quantum efficiency, and the photoelectron count is multiplied by the PMT gain with its variance inflated by an excess noise factor. The resulting charge is integrated on the preamplifier feedback capacitance and decays through the feedback resistance, giving a pulse with a fast rise set by the scintillation decay and an exponential fall set by the preamplifier time constant τ. Electronic noise and mains pickup are added before the trace is sampled and quantised by a modelled analogue-to-digital converter (ADC). All random streams are seeded, so every result in this paper can be regenerated exactly. Multiple Compton scattering, scintillator non-proportionality and temperature dependence are not modelled.

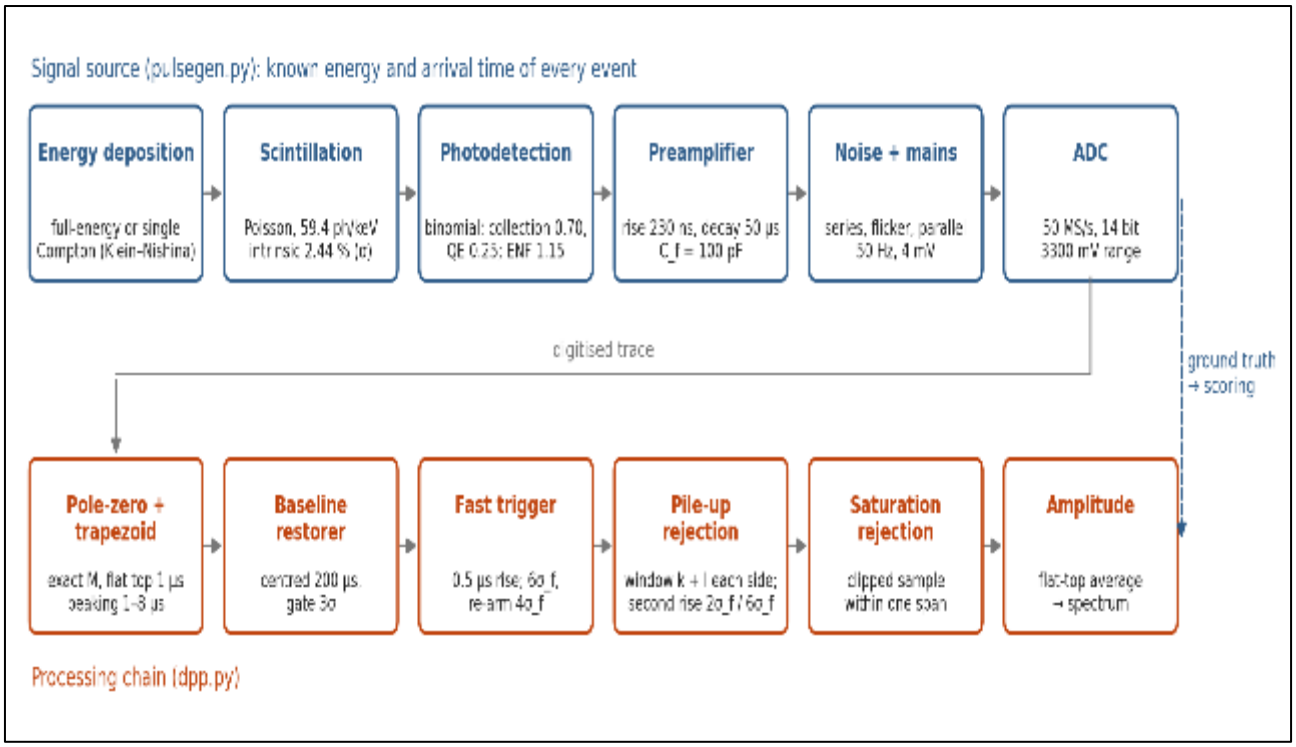


Figure 1: The framework. Top: the signal source, stage by stage, with the model's default values (read from the code). Bottom: the processing chain. The digitised trace links them; the known energy and arrival time of every event (dashed) is what each result is scored against

2.1.2 Calibration

The light yield is set to 59.4 photons/keV, the highest value Luan et al. measured with the single-photoelectron technique among 35 NaI(Tl) samples; small bare samples gave 50–60 photons/keV, and larger or encapsulated crystals less [26]. It is therefore a high-end value for a small bare crystal. The model is calibrated to the 6.5 % full width at half maximum (FWHM) at 662 keV that Dorenbos et al. report for a Ø25 × 12.5 mm NaI(Tl) crystal, which they divide into a photoelectron-statistics term $R_M = 3.1\,\%$ and a scintillator term $R_s = 5.7\,\%$ [27]. With the adopted light yield the model's statistical term is 3.04 % FWHM, so the intrinsic scintillator broadening was set to 2.44 % (σ), or 5.75 % FWHM, giving $\sqrt{3.04^2 + 5.75^2} = 6.5\,\%$. The two terms correspond closely to R_M and R_s. An independent measurement agrees: Moszyński et al. found an intrinsic resolution of 5.8 ± 0.24 % FWHM at 661.6 keV for a Ø10 × 10 mm crystal, with only the photomultiplier statistics removed [28]. Because R_s includes non-proportionality, crystal inhomogeneity and light-transfer fluctuations, the term is called intrinsic scintillator broadening rather than non-proportionality broadening. Only the 662 keV point is calibrated; the model's resolution at other energies follows from the assumption that this term does not depend on energy.

2.1.3 Headroom and count-rate ceiling

The higher light yield increases the charge per keV, so the feedback capacitance was raised to 100 pF. The 662 keV pulse then peaks at 97.5 % of its charge step, because the 50 µs decay starts during the 230 ns rise, and the energy whose mean pulse just reaches the ADC full-scale input (3099.8 mV above the 200 mV offset) is about 1910 keV, above the 1461 keV ^{40}K line.

That headroom applies to a single pulse on a quiet baseline. The modelled preamplifier has resistive feedback and is DC-coupled to the ADC, so at rate the decaying tails stack [29]. Its average output level is set by the input current [30], and random arrivals make the level fluctuate about that average, so any finite ADC range is eventually exceeded [30]. In the model clipping therefore has no sharp onset: the fraction of 662 keV events whose own peak reaches full scale is about 0.02 % at 2 kcps, 0.95 % at 8 kcps, 1.8 % at 10 kcps and 12 % at 20 kcps (0.06 % at 10 kcps for a full ^{137}Cs spectrum, whose average pulse is smaller). About 10 kcps is taken as the modelled front end's count-rate ceiling. This is a property of the modelled analogue front end, not of the processing chain.

2.1.4 Noise model

Three noise processes and a deterministic mains term are added to the preamplifier output. Series (white) noise is independent from sample to sample and represents the preamplifier's input voltage noise; its contribution after shaping

falls as $1/\sqrt{t_p}$ with peaking time t_p. Flicker noise is generated with a $1/\sqrt{f}$ amplitude spectrum; its contribution is roughly independent of t_p. Parallel noise is white noise low-pass filtered with the preamplifier's own time constant, representing leakage-current shot noise integrated on the feedback capacitance; its contribution rises as $\sqrt{t_p}$. These are the rms forms of the standard equivalent-noise-charge scaling [13, 14]. Mains pickup is a 50 Hz sinusoid (the Nigerian grid frequency) of 4 mV amplitude with random phase per trace. Two front ends are defined, differing only in series and parallel noise (Table 1): a nominal front end representative of a well-matched PMT preamplifier, and a low-cost front end representative of inexpensive discrete electronics. All noise amplitudes are assumptions chosen so that the two front ends differ; none is taken from a datasheet or a measured circuit.

Table 1: Principal model parameters. "Sourced" values are taken from, or bounded by, the cited measurement; "assumed" values are design choices of this study

Parameter	Value	Basis
Light yield	59.4 photons/keV	Sourced: highest measured value [26]
Scintillation decay	230 ns	Sourced [31]
PMT quantum efficiency	0.25	Sourced, rounded down: bialkali 27 % peak, ≈ 26 % at 420 nm [32]
Light-collection efficiency	0.70	Assumed; with the quantum efficiency, it sets the photoelectron number (6881 at 662 keV) and hence the statistical term of the energy resolution
PMT gain	10^5	Assumed; with C_f it sets the pulse height per keV
Excess noise factor	1.15	Assumed, within the measured range ε = 0.09–0.19 [28]
Preamplifier decay τ	50 µs	Assumed; same order as an HPGe preamplifier [33]
Feedback capacitance	100 pF	Derived from light yield and ADC range
Sampling rate; ADC	50 MS/s; 14 bit, 3300 mV, 200 mV offset	Assumed
Intrinsic scintillator broadening	2.44 % σ (5.75 % FWHM)	Calibrated to 6.5 % at 662 keV [27]
Series noise (nominal / low-cost)	2 / 55 mV rms	Assumed
Parallel noise (nominal / low-cost)	12 / 30 mV rms	Assumed
Flicker noise	1 mV	Assumed, both front ends
Mains pickup	50 Hz, 4 mV	Assumed

2.2 The pulse processing chain

The chain processes each digitised trace offline in six stages. Shaping follows the recursive formulation of Jordanov and Knoll [5]; event detection uses a separate fast filter, following the fast/slow architecture of Warburton et al. [6].

2.2.1 Pole-zero cancellation and trapezoidal shaping

Pole-zero cancellation and trapezoidal shaping are implemented as a single recursion [5], in the form

$$d[n] = v[n] - v[n-k] - v[n-\ell] + v[n-k-\ell], \quad p[n] = p[n-1] + d[n],$$

$$r[n] = p[n] + M\,d[n], \quad s[n] = s[n-1] + r[n],$$

[11], where k is the peaking time in samples and $\ell = k$ + flat top. The pole-zero parameter is used in its exact discrete form, $M = 1/\left(e^{T/\tau} - 1\right)$ [11], where T is the sampling period. Applying the running sum plus M times the input to a sampled exponential Ab^n, $b = e^{-T/\tau}$, gives a step of height $A/(1-b)$ plus a residual tail proportional to $M - b/(1-b)$, which vanishes for the exact M. Expanding to second order gives $M \approx \tau/T - 1/2$, the approximation Jordanov et al. give

for $\tau/T > 5$; the cruder $M \approx \tau/T$ of [5] keeps only the first-order term. Because $M + 1 = 1/(1 - b)$, the flat-top height for a unit-amplitude exponential input is $k(M + 1)$: this is Jordanov's unfolding factor $1/(1 - a)$ [12] combined with the k-sample rise of the trapezoid. The chain divides by $k(M + 1)$ so that amplitudes are reported in input millivolts. This amplitude calibration is not the filter's gain at zero frequency. Writing the recursion as $H(z) = (1 - z^{-k})\big(1 - z^{-\ell}\big)[1 + M(1 - z^{-1})]/(1 - z^{-1})^2$ and letting $z \to 1$ gives $H(1) = k\ell$; normalised by $k(M + 1)$, a slow input passes at $\ell/(M + 1) \approx \big(t_p + \text{flat top}\big)/\tau$. The recursion costs seven arithmetic operations per sample, independent of peaking time, with a delay line of $k + \ell$ samples.

2.2.2 Baseline restoration

A trapezoidal filter's weight function has finite area, so it does not reject a constant input current [19], and the pole-zero stage reads a steady preamplifier level as such a current. The deconvolution reduces an offset or drift but does not remove it [20]; the pole-zero stage used here is that deconvolution scaled by $M + 1$, since $1 + M(1 - z^{-1}) = (M + 1)(1 - bz^{-1})$. Slow signals, together with the low-frequency wander of parallel noise, are therefore removed by a separate restorer. It estimates the baseline as a moving average over a centred 200 µs window of the shaped output, using only samples within 3σ of zero (σ from the median absolute deviation), so that pulses do not bias the estimate. Estimates taken symmetrically before and after a pulse average to the value of a ramp at the pulse [19], so a linear drift is removed without bias. The centred window uses future samples and so suits offline processing only.

2.2.3 Fast-channel trigger

Events are detected on a short second trapezoid (0.5 µs rise, 0.2 µs flat top, same pole-zero correction) rather than on the slow energy filter, whose threshold crossing time depends on pulse height [13, 14]. A trigger is a rising crossing of $6\sigma_f$, where σ_f is the fast filter's noise estimated by the median absolute deviation, followed by a hold-off of one fast span (1.2 µs). Because the 230 ns scintillation tail follows the fast trapezoid, a 662 keV fast pulse stays above threshold for longer than the hold-off, so the channel is re-armed only once the fast output has fallen below $4\sigma_f$. This is ordinary comparator hysteresis, as in a Schmitt trigger. Each event's start time is then estimated by half-height timing (the first sample at or above half of the fast pulse's local maximum, stepped back by half the fast rise time) which is constant-fraction timing at a fraction of 0.5 and is independent of pulse height for a linear filter [14].

2.2.4 Pile-up rejection

An event with another fast trigger within one slow span, $k + \ell$ samples, on either side is discarded and counted as dead time. For Poisson arrivals at rate R the expected rejected fraction is

$$P = 1 - \exp[-2R(k + \ell)/f_s],$$

from the probability of no further event in a window of $k + \ell$ samples on each side [34]. Because an event is rejected regardless of whether its neighbour is kept, the rule is an extendable dead time, and the expected throughput $R\exp[-2R(k + \ell)/f_s]$ has the paralysable form $m = ne^{-n\tau_d}$ [17] with $\tau_d = 2(k + \ell)/f_s$, as shown for pile-up rejection by Pommé et al. [18].

Rejection can only act on triggers it is given. A second pulse that arrives while the first is still above threshold makes no new rising crossing. The chain therefore also inspects each fast pulse for a second rise: if the output, having fallen at least $2\sigma_f$ below its running peak, then climbs more than $6\sigma_f$ above its lowest value since, a second pulse is declared and added as a trigger, so that both pulses are rejected. The principle (a fall by more than a noise-set margin followed by a renewed rise while the signal is still above threshold) is that of Mott's pile-up detector, which applies it to a digital estimate of the preamplifier signal's slope [15]; here it is applied to the fast-trapezoid output, with separate fall and rise margins.

2.2.5 Saturation rejection and amplitude measurement

An event with a full-scale ADC sample within one slow span of its start is discarded and counted separately. For the remaining events the slow trapezoid's flat top is averaged over its central region, with a guard fraction trimmed from each end, starting from the fast-channel time estimate, and the amplitudes are histogrammed. Figure 2 shows the stages on 600 µs of modelled trace.

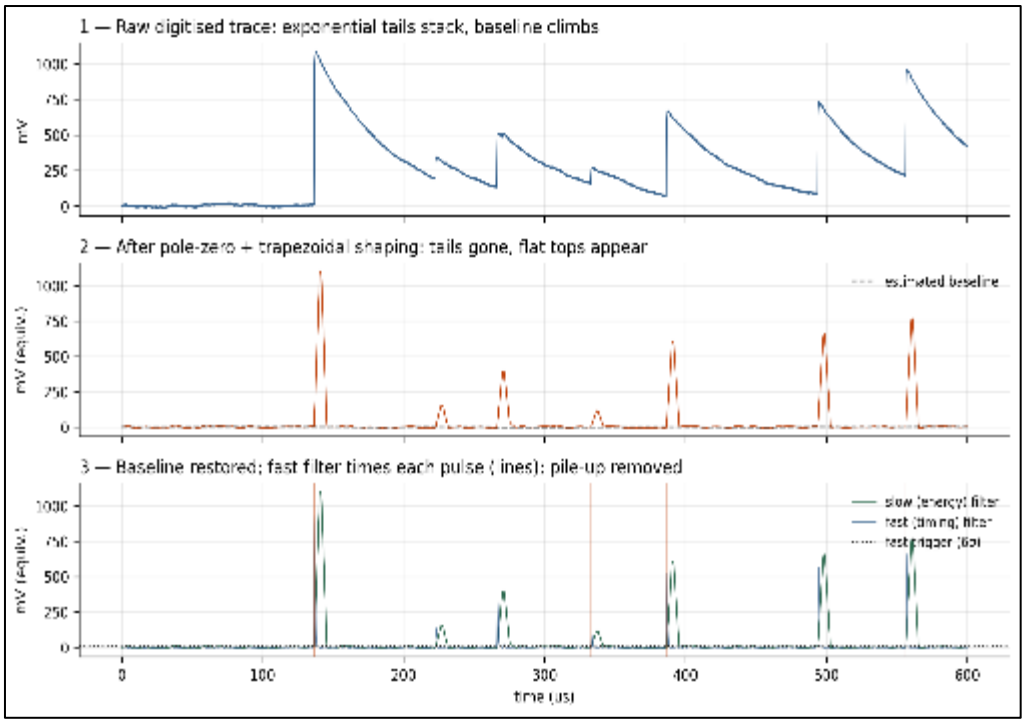


Figure 2: The chain applied to 600 µs of modelled trace (^{137}Cs at 8 kcps, nominal front end, 4 µs peaking time, 1 µs flat top). Top: the digitised preamplifier output, where each pulse rides on the tails of earlier ones. Middle: after pole-zero cancellation and trapezoidal shaping, with the estimated baseline (dashed). Bottom: the slow (energy) and fast (timing) filter outputs and the fast trigger threshold (dotted); vertical lines mark the events that survive pile-up and saturation rejection. All eight events trigger; the two near 270 µs lie within one slow span of each other and are both rejected, leaving six measured

2.3 Verification approach

Each test in the Results states what is tested, against what reference, and the result. Three kinds of reference are used, and they are not equivalent: the generator's own ground truth (event energies and arrival times), closed-form expressions derived for this recursion, and published measurements or theory. Every result is obtained from modelled signals. Some analysis and plotting scripts were written with the help of an AI assistant (Claude by Antropic), every script was run on the corresponding author's computer, and the processing chain and signal model were designed and verified by the corresponding author.

3 RESULTS AND DISCUSSION

The results in this section verify the framework against the references described above; none is a measurement on a physical detector.

3.1 Pulse shape

Reference: analytical single-pole rise; configured τ. For one noiseless 662 keV event the 10–90 % rise time is 460 ns, shorter than the 505 ns (2.197 × 230 ns) of a pure single-pole rise because the 50 µs decay is already under way while the pulse rises. An exponential fitted to the tail returns 50.00 µs, the configured value (Figure 3).

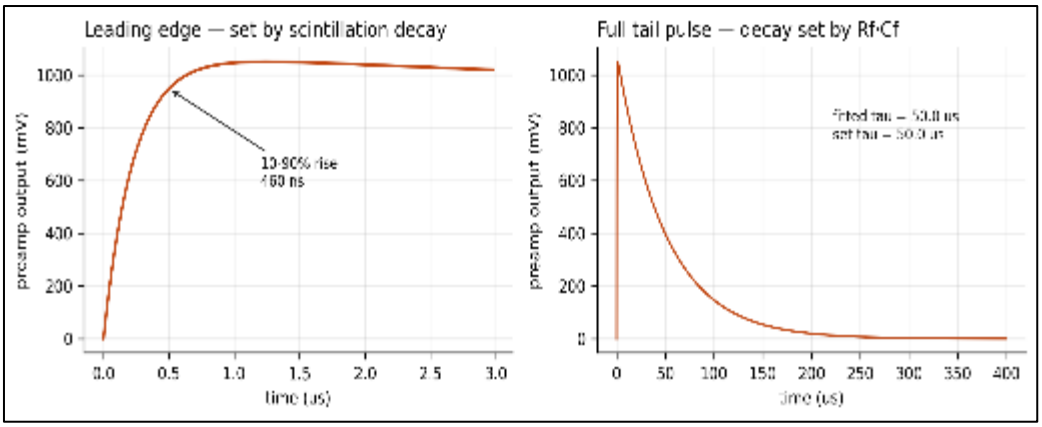


Figure 3: Modelled preamplifier output for one 662 keV event, without noise. Left: the leading edge; its 10–90 % rise time is 460 ns, shorter than the 505 ns of a pure single-pole rise because the 50 µs decay is already under way. Right: the full pulse; an exponential fitted to the tail returns the configured 50.0 µs

3.2 Detector model

Reference: published resolution at one energy. Before electronic noise, shaping and digitisation, the modelled photopeak has 6.50 % FWHM at 662 keV, the calibration target. This agreement is imposed by calibration and is not an independent validation. At 60 keV and 1332 keV the model gives 11.59 % and 6.13 %. These are consequences of the energy-independent intrinsic term, which keeps the model below a pure $1/\sqrt{E}$ curve through the 662 keV point at low energy and above it at high energy; they have not been compared with a measurement (Figure 4).

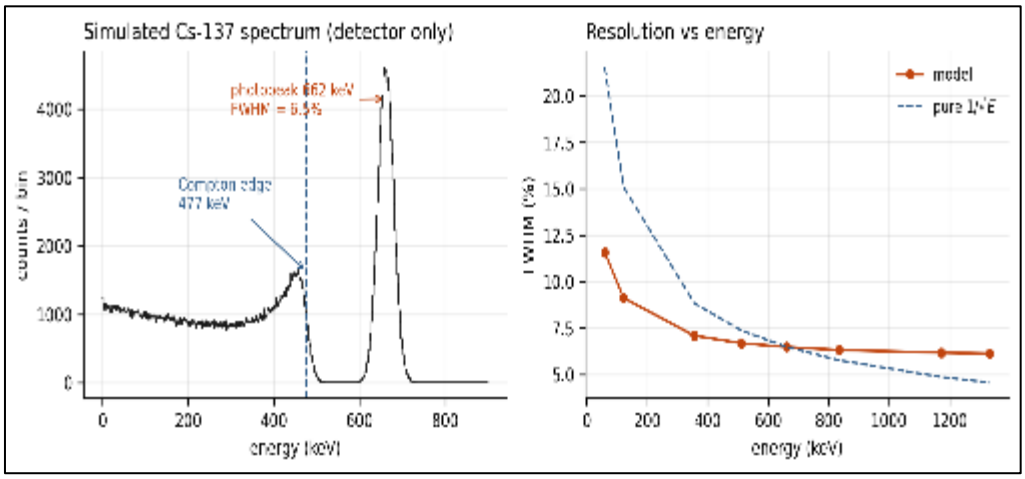


Figure 4: The modelled detector alone, before electronic noise, shaping and digitisation. Left: simulated ^{137}Cs spectrum, with the Compton edge at 477 keV and the 662 keV photopeak at 6.5 % FWHM, the calibration target; each event is a full-energy deposit or a single Compton scatter, so the region between the edge and the photopeak is empty. Right: photopeak FWHM against energy, with a pure $1/\sqrt{E}$ curve through the 662 keV point. Only the 662 keV value is calibrated against a published measurement

3.3 Amplitude calibration and the pole-zero constant

Reference: closed-form results for this recursion. For an ideal 50 µs exponential with $k = 200$, $\ell = 250$ at 50 MS/s, the measured flat top divided by $k(M + 1)$ is 1.0000000000000; dividing by kM instead overstates the amplitude by a factor 1.0004, that is by $1/M$. At this operating point ($\tau/T = 2500$) the exact M is 2499.500033: the approximation $M \approx \tau/T$ is high by a relative 2.00×10^{-4} and $M \approx \tau/T - 1/2$ is low by 1.3×10^{-8}, the size of the next term of the series, $T/(12\tau)$, relative to M. At $\tau/T = 5$ the same errors are 10.7 % and 0.37 %. Applied to a sampled exponential over 8τ, the pole-zero stage with the exact M holds the step height to within 6×10^{-14} (floating-point rounding); with $M = \tau/T$ the output starts high by a relative 2.0×10^{-4} and the excess decays with the preamplifier's own time constant, as the residual-tail term predicts. At 50 MS/s the exact form is therefore not needed for accuracy (using $M = \tau/T$ is equivalent to a 0.02 % error in τ) but it stays correct when τ/T is small, for a short decay or slow sampling.

3.4 Mis-set pole-zero constant

Reference: expected sign of the residual tail. A single 662 keV pulse shaped with τ set 40 % low over-corrects the decay: the flat top slopes upward and the tail overshoots the baseline. With τ set 60 % high it under-corrects: the flat top sags and the tail undershoots (Figure 5). This is the signature used in practice to set the constant, by checking that the flat top runs parallel to the baseline [20]. The test is qualitative.

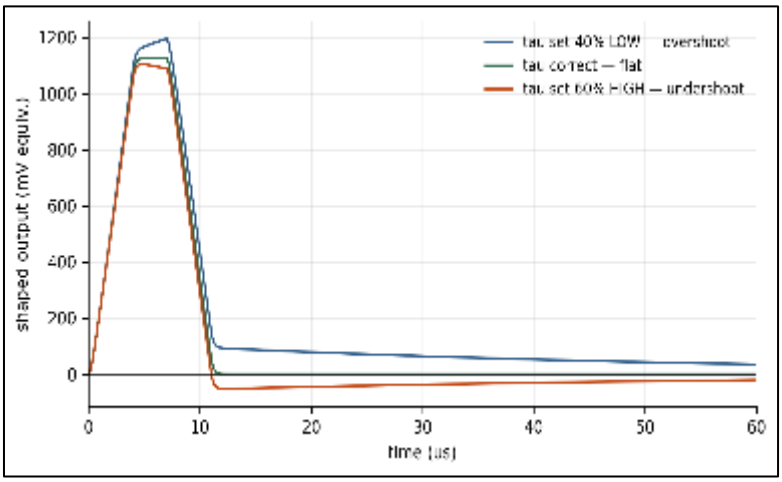


Figure 5: A single 662 keV pulse shaped with the preamplifier decay constant τ set correctly, 40 % too low (over-correction: the flat top slopes up and the tail overshoots) and 60 % too high (under-correction: the flat top sags and the tail undershoots)

3.5 Low-frequency behaviour

References: the closed-form pass-through $\ell/(M+1)$; the restorer's own transfer function; and Pullia et al.'s analysis of baseline estimates.

Shaper. With a constant or slowly varying input, the shaper output settles at $\ell/(M+1)$ of the input: 0.09998 at 4 µs peaking and 1 µs flat top, and 0.33993 at 16 µs, matching the closed form. A non-zero plateau is the expected behaviour of a finite-area (unipolar) shaper [19, 20], and Wang et al. plot such a plateau for the Jordanov filter [35]; the closed form $\ell/(M+1)$ for this recursion is derived here. At the trapezoid geometry of Pullia et al.'s measurements (10 µs total, 1.6 µs flat top) [19] the plateau is 0.1160 against $\ell/(M+1) = 0.11598$, and with injected sinusoids from 50 Hz to 10 kHz it rises as $\ell/(M+1)\,|1 + j2\pi f\tau|$ to within 1 % up to about 5 kHz (0.8 % low at 10 kHz).

Restorer. With its gate held open and no pulses, the centred 200 µs restorer is a linear filter whose gain should be $1 - \mathrm{sinc}(fW)$, $W = 200$ µs. Measured gains agree with this to within 0.0016 dB from 50 Hz to 10 kHz, with −75.7 dB at 50 Hz. This confirms that the restorer is implemented as intended; it is not a comparison with Pullia et al., whose two-lobe model, with lobes 200 µs from the pulse, gives −54.1 dB at 50 Hz. The two are not like for like: the window here is centred on the pulse, and estimates nearer the pulse reject slow signals better.

Centred vs trailing window. Pullia et al. show that a single baseline estimate taken before the pulse leaves a first-order zero at zero frequency (20 dB per decade), whereas symmetric estimates give a second-order zero (40 dB per decade) [19]. Replacing the centred window by a trailing (causal) 200 µs window reproduces this: the slopes are 40 and 20 dB per decade, and the rejection at 50 Hz falls from −75.7 dB to −30.1 dB. For the 4 mV mains term, which leaves about 0.4 mV after shaping, a trailing window would leave about 13 µV after restoration — far below the shaped noise (the restorer's 3σ gate is 14–61 mV for both front ends at 4 and 16 µs). This test shows the qualitative prediction holds for this chain; the absolute dB values are specific to the 200 µs window.

4 DISCUSSION

What the framework is for. The framework lets a processing chain for a low-cost NaI(Tl) spectrometer be designed and tested before any detector or digitiser is available, and lets each stage be judged event by event rather than only through the final spectrum. Every result can be regenerated from the seeded code, which also makes the framework usable for teaching: a student can change one stage and see exactly which events it gains or loses. For laboratories like those described in the Introduction, where equipment is the constraint, this moves much of the design work onto an ordinary computer.

Lessons for low-cost designs. Two follow from the results and are specific to the chain tested here.

- The baseline restorer is load-bearing, not optional. A trapezoidal shaper passes slow signals at $\ell/(M + 1)$ of their size, about 10 % at 4 μs peaking and 1 μs flat top, so mains pickup, drift and parallel-noise wander reach the amplitude measurement unless a later stage removes them.
- A real-time system needs a causal (trailing) baseline window. At the 200 μs window used here this costs about 45 dB of rejection at 50 Hz, but at the modelled mains level the residue after restoration is about 13 μV, far below the shaped noise. The loss would matter only if pickup were hundreds of times larger than modelled: 13 μV is about 1/360 of the shaped noise σ, 4.7 mV, on the nominal front end at 4 μs *(own calculation; σ is one third of the 14 mV gate)*.

Limitations. All results in this paper are obtained from modelled signals; the chain has not been tested on waveforms recorded from a physical detector. The 6.5 % resolution at 662 keV is the model's calibration target and is not an independent test. Validation on measured waveforms, which would require a digitiser and detector or a public raw-waveform dataset matching the modelled front end, is future work. Within the model: energy deposition is limited to full-energy and single-Compton events; scintillator non-proportionality and temperature dependence are not modelled; the electronic-noise amplitudes, the light-collection efficiency and the PMT gain are assumptions, not measured values (Table 1); and arrivals are purely Poisson. The low-frequency tests of the restorer hold the gate open and contain no pulses. The trigger, the pile-up rejection and the gated restorer are described here, but their measured performance on pulses, close pairs and drift is not reported in this paper. The chain is implemented in Python and run offline; its computational cost is not evaluated here.

5 CONCLUSION

A seeded, physics-based model of a NaI(Tl)/photomultiplier/preamplifier front end, calibrated to a published resolution, has been paired with a digital pulse-processing chain built from established techniques, so that every stage can be scored against the known energy and arrival time of each event. The chain reproduces its closed-form behaviour to within the precision tested, and its centred and trailing baseline estimates follow the published 40 and 20 dB-per-decade prediction. All results are modelled. The chain's measured limits and performance are reported separately, and testing it on recorded detector waveforms remains future work.

STATEMENTS ON COMPLIANCE WITH ETHICAL STANDARDS

Acknowledgments

The authors are grateful to A. Temirzhanov for kindly sharing the pre-proof of his group's article on a microcontroller-based digital spectrometer before its publication. The authors also thank the Department of Physics, Federal University Otuoke, for its unrelenting support and its push for excellence. This research received no specific grant from any funding agency.

Disclosure of conflict of interest

The authors declare no conflict of interest.

Code and data availability

The source code of the signal model (pulsegen.py) and the processing chain (dpp.py), every script that produces a number or figure in this paper, and the result files they write are available at https://github.com/humphreyayodele/gamma-dpp-chain and archived at 10.5281/zenodo.24147429; the code is released under the MIT licence and the result files under CC BY 4.0. The README of the repository lists the script and output file behind each figure and number. All random streams are seeded; each script states its seeds, and re-running it reproduces the published values exactly on the same software versions (Python 3.13.7, NumPy 2.4.2, SciPy 1.17.0, pandas 3.0.1, Matplotlib 3.10.8).

Author contributions

Uzo Anekwe: supervision, writing (review and editing). Humphrey Ayodele Peleyeju: conceptualisation, methodology, software, investigation, formal analysis, writing (original draft, review and editing). Chibuzo Emeruwa: writing (review and editing).

REFERENCES

[1] Avwiri GO, Esi E, Agbalagba EO. Gamma spectroscopy analysis of produced water from selected flow stations in Delta State, Nigeria. International Journal of Environmental Monitoring and Analysis. 2013;1(5):167–174. doi:10.11648/j.ijema.20130105.11

[2] Agbalagba EO, Avwiri GO, Chad-Umoreh YE. γ-Spectroscopy measurement of natural radioactivity and assessment of radiation hazard indices in soil samples from oil fields environment of Delta State, Nigeria. Journal of Environmental Radioactivity. 2012;109:64–70. doi:10.1016/j.jenvrad.2011.10.012

[3] Anekwe UL, Uzoekwe SA, Ibe SO. Estimation of health risks in borehole water supply, case study in Ogbia, Nigeria. OSP Journal of Health Care and Medicine. 2023;4(1):1–8. Article HCM-4-142.

[4] Babatunde BB, Sikoki FD, Avwiri GO, Chad-Umoreh YE. Review of the status of radioactivity profile in the oil and gas producing areas of the Niger delta region of Nigeria. Journal of Environmental Radioactivity. 2019;202:66–73. doi:10.1016/j.jenvrad.2019.01.015

[5] Jordanov VT, Knoll GF. Digital synthesis of pulse shapes in real time for high resolution radiation spectroscopy. Nuclear Instruments and Methods in Physics Research A. 1994;345(2):337–345. doi:10.1016/0168-9002(94)91011-1

[6] Warburton WK, Momayezi M, Hubbard-Nelson B, Skulski W. Digital pulse processing: new possibilities in nuclear spectroscopy. Applied Radiation and Isotopes. 2000;53(4–5):913–920. doi:10.1016/S0969-8043(00)00247-5

[7] Cao VH, Dinh TH, Nguyen TT, Nguyen KH, Pham DK, Nguyen XH, et al. Flexible and low-cost FPGA-based multichannel analyzer for handheld measurement devices. Nuclear Instruments and Methods in Physics Research A. 2021;1018:165808. doi:10.1016/j.nima.2021.165808

[8] Jana A, Singh SK, Gupta A, Das S, Basu K, Samanta S, et al. Development of a zero-cost multichannel analyser based on digital signal processing for γ-ray spectroscopy using the PC sound card. Pramana – Journal of Physics. 2020;94:20. doi:10.1007/s12043-019-1880-6

[9] Inoue K, Fukushi M, Van Le T, Tsuruoka H, Kasahara S, Nimelan V. Distribution of gamma radiation dose rate related with natural radionuclides in all of Vietnam and radiological risk assessment of the built-up environment. Scientific Reports. 2020;10:12428. doi:10.1038/s41598-020-69003-0

[10] Saint-Gobain Crystals. Low level/low background counting. Detector applications information note, rev. 08-16 [Internet]. Saint-Gobain Ceramics & Plastics; 2016 [cited 2026 Oct 20]. Available from: https://luxiumsolutions.com/sites/default/files/2021-11/Low-Level-Low-Background-Counting-Application.pdf

[11] Jordanov VT, Knoll GF, Huber AC, Pantazis JA. Digital techniques for real-time pulse shaping in radiation measurements. Nuclear Instruments and Methods in Physics Research A. 1994;353(1–3):261–264. doi:10.1016/0168-9002(94)91652-7

[12] Jordanov VT. Unfolding-synthesis technique for digital pulse processing. Part 1: Unfolding. Nuclear Instruments and Methods in Physics Research A. 2016;805:63–71. doi:10.1016/j.nima.2015.07.040

[13] Spieler H. Electronics. In: Grupen C, Shwartz B. Particle Detectors. 2nd ed. Cambridge: Cambridge University Press; 2008 (reissued open access 2023). p. 390–435. doi:10.1017/9781009401531.017

[14] Sadrozinski HF-W, Seiden A, Cartiglia N. 4-Dimensional tracking with ultra-fast silicon detectors. arXiv:1704.08666v4 [physics.ins-det] [Preprint]. 2017. doi:10.48550/arXiv.1704.08666

[15] Mott RB. Pileup rejection in an energy-dispersive radiation spectrometry system. United States patent US 7,763,859 B2. 2010.

[16] Manton JH. Pulse processing — overview and challenges. Signal Processing. 2025;234:109978. doi:10.1016/j.sigpro.2025.109978

[17] Usman S, Patil A. Radiation detector deadtime and pile up: a review of the status of science. Nuclear Engineering and Technology. 2018;50(7):1006–1016. doi:10.1016/j.net.2018.06.014

[18] Pommé S, Denecke B, Alzetta J-P. Influence of pileup rejection on nuclear counting, viewed from the time-domain perspective. Nuclear Instruments and Methods in Physics Research A. 1999;426(2–3):564–582. doi:10.1016/S0168-9002(99)00016-9

[19] Pullia A, Gritti G, Ripamonti G. Design of high performance digital baseline restorers. IEEE Transactions on Nuclear Science. 1997;44(3):331–337. doi:10.1109/23.603665

[20] Zeng G, Yang J, Hu T, Ge L, Ouyang X, Zhang Q, et al. Baseline restoration technique based on symmetrical zero-area trapezoidal pulse shaper. Nuclear Instruments and Methods in Physics Research A. 2017;858:57–61. doi:10.1016/j.nima.2017.03.049

[21] Radeka V. Effect of "baseline restoration" on signal-to-noise ratio in pulse amplitude measurements. Review of Scientific Instruments. 1967;38(10):1397–1403. doi:10.1063/1.1720548

[22] Geraci A, Rech I, Gatti E, Ripamonti G. Shared baseline restoration at minimum noise for high resolution spectroscopy. Nuclear Instruments and Methods in Physics Research A. 2002;482:441–448. doi:10.1016/S0168-9002(01)01509-1

[23] Wen X, Wei Y. Optimum digital filters for baseline restoration. IEEE Transactions on Nuclear Science. 2006;53(6):3865–3869. doi:10.1109/TNS.2006.884096

[24] Ibrahim MM, Yussup N, Lombigit L, Rahman NAA, Jaafar Z. Development of multichannel analyzer using sound card ADC for nuclear spectroscopy system. AIP Conference Proceedings. 2014;1584:50–53. doi:10.1063/1.4866103

[25] Temirzhanov A, Sadykov BM, Zholdybayev TK, Duisebayev BA, Berikov D, Issatayev T, et al. Real-time digital pulse processing for alpha spectroscopy using a low-cost 32-bit microcontroller. Nuclear Instruments and Methods in Physics Research A. 2026. In press. doi:10.1016/j.nima.2026.171710

[26] Luan NT, Kim HJ, Lee HS, Jegal J, Truc LT, Khan A, et al. Absolute light yield measurement of NaI:Tl crystals for dark matter search. arXiv:2404.18551v1 [Preprint]. 2024. doi:10.48550/arXiv.2404.18551

[27] Dorenbos P, de Haas JTM, van Eijk CWE. Non-proportionality in the scintillation response and the energy resolution obtainable with scintillation crystals. IEEE Transactions on Nuclear Science. 1995;42(6):2190–2202. doi:10.1109/23.489415

[28] Moszyński M, Zalipska J, Balcerzyk M, Kapusta M, Mengesha W, Valentine JD. Intrinsic energy resolution of NaI(Tl). Nuclear Instruments and Methods in Physics Research A. 2002;484:259–269. doi:10.1016/S0168-9002(01)01964-7

[29] Landis DA, Goulding FS, Pehl RH, Walton JT. Pulsed feedback techniques for semiconductors detector radiation spectrometers. Report UCRL-20151 [Internet]. Berkeley: Lawrence Radiation Laboratory, University of California; 1970. Available from: https://escholarship.org/uc/item/02k798cv

[30] Warburton WK, Hubbard B. Method and apparatus for analog signal conditioner for high speed, digital x-ray spectrometer. United States patent US 5,870,051. 1999.

[31] Di Fulvio A, Shin TH, Hamel MC, Pozzi SA. Digital pulse processing for NaI(Tl) detectors. Nuclear Instruments and Methods in Physics Research A. 2016;806:169–174. doi:10.1016/j.nima.2015.09.080

[32] Hamamatsu Photonics K.K. Photomultiplier Tubes: Basics and Applications. 4th ed. Hamamatsu: Hamamatsu Photonics K.K.; 2017.

[33] Salathe M, Kihm T. Optimized digital filtering techniques for radiation detection with HPGe detectors. Nuclear Instruments and Methods in Physics Research A. 2016;808:150–155. doi:10.1016/j.nima.2015.11.051

[34] Grupen C, Shwartz B. Characteristic properties of detectors. In: Particle Detectors. 2nd ed. Cambridge: Cambridge University Press; 2008 (reissued open access 2023). p. 56–70. doi:10.1017/9781009401531.005

[35] Wang H-P, Zhou J-B, Ouyang X-P, Tuo X-G, Hong X, Liu Y, et al. Application of pole-zero cancellation circuit in nuclear signal filtering and shaping algorithm. Nuclear Science and Techniques. 2021;32:86. doi:10.1007/s41365-021-00916-9